



Contents lists available at ScienceDirect

# Mechanical Systems and Signal Processing

journal homepage: [www.elsevier.com/locate/ymsp](http://www.elsevier.com/locate/ymsp)

## Study on Hankel matrix-based SVD and its application in rolling element bearing fault diagnosis



Huiming Jiang\*, Jin Chen, Guangming Dong, Tao Liu, Gang Chen

State Key Laboratory of Mechanical System and Vibration, Shanghai Jiao Tong University, No. 800, Dongchuan Road, Shanghai 200240, China

### ARTICLE INFO

#### Article history:

Received 21 October 2013

Received in revised form

14 July 2014

Accepted 26 July 2014

Available online 22 September 2014

#### Keywords:

Hankel matrix-based SVD

Singular value

Ratio of neighboring singular values

Continuous hidden Markov model

Rolling element bearing fault diagnosis

Performance degradation assessment

### ABSTRACT

Based on the traditional theory of singular value decomposition (SVD), singular values (SVs) and ratios of neighboring singular values (NSVRs) are introduced to the feature extraction of vibration signals. The proposed feature extraction method is called SV–NSVR. Combined with selected SV–NSVR features, continuous hidden Markov model (CHMM) is used to realize the automatic classification. Then the SV–NSVR and CHMM based method is applied in fault diagnosis and performance assessment of rolling element bearings. The simulation and experimental results show that this method has a higher accuracy for the bearing fault diagnosis compared with those using other SVD features, and it is effective for the performance assessment of rolling element bearings.

© 2014 Elsevier Ltd. All rights reserved.

### 1. Introduction

Rolling element bearings find widespread industrial applications and their failures cause malfunctions and may even lead to catastrophic failure of the machinery [1]. Hence, vibration signals generated by faults in bearings have been widely studied and a lot of research work on bearing fault diagnosis has been published [2]. In general, fault diagnosis can be regarded as a problem concerning pattern identification which mainly includes two important procedures: feature extraction and pattern classification [3]. In order to acquire more fault information from vibration signals and improve the accuracy of the diagnosis work, many feature extraction methods have been proposed, such as wavelet transform [4–6], empirical mode decomposition [7–10], multi-scale entropy [11–14] and so on.

Singular value decomposition (SVD) is a non-parametric technique which has been widely used in feature extraction. The one-dimensional signal can be transformed into many kinds of matrices, such as Toeplitz matrix, cycle matrix and Hankel matrix. Zhao et al. pointed out that the signal processing effect of Hankel matrix-based SVD was very similar to that of wavelet transform [15]. The similarity of Hankel matrix-based SVD and wavelet transform in signal processing could be applied to noise reduction, singularity detection, feature extraction and fault diagnosis. Liu chose singular values (SVs) obtained by Hankel matrix-based SVD as features for bearing fault diagnosis [16], where the SV features combined with continuous hidden Markov model (CHMM), were shown effective in bearing fault diagnosis and performance assessment. In references [17,18], singular value ratio (SVR) spectrum was introduced to detect the periodicity in signal. Cong introduced SVR and short-time matrix series to vibration signal processing [19], which had a good local identification capability in the rolling bearing fault diagnosis. In most of these literatures, SVs and SVR were extracted as features for further learning. In this paper, a new feature extraction method based on SVD is proposed. SVs and ratios of neighboring

\* Corresponding author.

E-mail address: [qmihu@hotmail.com](mailto:qmihu@hotmail.com) (Huiming Jiang).

singular values (NSVRs) which are obtained by Hankel matrix-based SVD are applied to the feature extraction of vibration signals. The proposed method is called SV–NSVR.

Pattern recognition is another key part of the intelligent vibration monitoring. Hidden Markov model (HMM), as one statistical method for pattern recognition, was initially introduced and studied in the late 1960s and early 1970s. HMM has been widely used in speech recognition [20] for decades. In recent years, HMM has been applied in many other fields, such as speaker recognition [21], handwriting recognition [22], biomedical signal processing [23], fault diagnosis [24], state prognosis [25] and so on. There are many extensions of HMM which have been applied to fault diagnosis. Li et al. proposed factorial hidden Markov model (FHMM) for the fault recognition of non-stationary processes [26]. Dong [27,28] presented a statistical modeling methodology based on segmental hidden semi-Markov models (HSMMS) for both diagnosis and prognosis in a unified framework. FHMM and HSMMS both overcame some inherent limitations of HMM technology, but the major drawback of them was that the computational complexity might increase for inference procedures and parameter estimations. Cartella et al. [29] combined left–right HMM with Change Point Detection (CPD) algorithms for bearings condition assessment, where improvements were made in terms of the reduction of training procedure iterations and early detection of unknown states compared with state of the art techniques. In their study, the state in the left–right HMM was detected by CPD algorithms. It was more adaptive for conditions with obvious segments such as the tool wearing and the drilling process. This paper focuses on a new feature extraction method and the verification of its performance combined with HMM. So the original hidden Markov model is utilized for automatic classification.

This paper is organized as follows: at first, the theory of Hankel matrix-based SVD is introduced. Then the SV–NSVR feature extraction method is proposed. The basic theory of CHMM is described in Section 3. Section 4 gives detailed procedures of applying SV–NSVR and CHMM to the bearing fault diagnosis and performance assessment. In Section 5, an artificial rolling element bearing fault experiment proves the effectiveness of the proposed method for fault diagnosis. In Section 6, an accelerated bearing life test is performed to show that the proposed method is valid for performance assessment. The conclusion of this paper is presented in Section 7.

## 2. Feature extraction based on SVD

Most of current feature extraction methods are complex in nature. Very few of them use a simple approach, and thus the further research towards developing a simple time series method for the bearing fault feature extraction is required [30]. SVD is a non-parametric technique and easy to implement which extracts the algebraic characteristic from data. The feature extraction and diagnosis based on SVD have many applications. Wang et al. [31] were the first to apply SVD to the diagnosis of machine failures using vibration signals. Muruganatham et al. applied SVD for decomposing the acquired bearing vibration signal into an additive set of time series to extract information for inner race bearing fault detection [32]. In reference [30], SVs and the energies of the principal components obtained from SVD were used as features for the bearing fault diagnosis. Because each principal component from SVD represented the different frequency spectrum of the signal [33] and SVs could be treated as projective coefficients of the original signal on new basis vectors to some extent, SVs and SVR were widely used as features for fault diagnosis [16,19]. SVR could be quite high if the signal was periodic with weak noise [17,18]. To the best of the authors' knowledge, other relationship between SVs has not been applied in the field of the bearing fault diagnosis so far. Its advanced properties attract us for a trial of its use. In this paper, the ratios between neighboring SVs are proposed as features for the bearing fault diagnosis. Singular values measure magnitudes of component signals to some extent. Each component signal represents a different spectrum component of the original signal [33]. So NSVRs can express relationships of different frequency components. SV–NSVRs are proposed as features for the bearing fault diagnosis and performance assessment in this paper. The detailed procedures are expressed in the following sections.

### 2.1. Singular value decomposition

The definition of SVD is, for a matrix  $A \in R^{m \times n}$ , there exist two orthogonal matrices:  $U=[u_1, u_2, \dots, u_m] \in R^{m \times m}$  and  $V=[v_1, v_2, \dots, v_n] \in R^{n \times n}$ , which meet the following equation:

$$A = U \Sigma V^T \tag{1}$$

where  $\Sigma = [\text{diag}(\sigma_1, \sigma_2, \dots, \sigma_q), 0]$  or its transposition, which is decided by whether  $m < n$  or  $m > n$ .  $\Sigma \in R^{m \times n}$ ,  $O$  is a zero matrix, and  $q = \min(m, n)$ . These parameters  $\{\sigma_i\}$  ( $i = 1, 2, \dots, q$ ) are called singular values (SVs) of  $A$ , and  $\sigma_1 \geq \sigma_2 \geq \dots \geq \sigma_q > 0$ .

### 2.2. SV–NSVR feature extraction

Vibration signals acquired from a rotating machine can always be expressed as time series. And the details of SVD can refer to references [15,16,32] and are described briefly as follows.

**Step 1: Embedding.** For a discrete signal  $X=[x(1), x(2), \dots, x(N)]$ , a Hankel matrix can be formed as

$$A = \begin{bmatrix} x(1) & x(2) & \cdots & x(n) \\ x(2) & x(3) & \cdots & x(n+1) \\ \vdots & \vdots & \vdots & \vdots \\ x(m) & x(m+1) & \cdots & x(N) \end{bmatrix} \tag{2}$$

$$A_i = \begin{pmatrix} \boxed{x_i(1)} & \boxed{x_i(2)} & \cdots & \boxed{x_i(n)} \\ x_i(2) & x_i(3) & \cdots & \boxed{x_i(n+1)} \\ \vdots & \vdots & \ddots & \vdots \\ x_i(m) & x_i(m+1) & \cdots & \boxed{x_i(N)} \end{pmatrix} \begin{matrix} R_{i,1} \\ \\ \\ C_{i,n} \end{matrix}$$

Fig. 1. The component matrix  $A_i$  when Hankel matrix is used.

where  $1 < m < N$ ,  $n = N - m + 1$  and  $A \in R^{m \times n}$ .  $m$  is the window length. The SVD performance depends on the window length and there are no standard rules for its choice [34]. With an appropriate  $m$ , the fault feature of the signal would be extracted more clearly [30]. So the choice of  $m$  is discussed through the experimental data.

**Step 2: Singular value decomposition.** From Eq. (2), the original signal can be described as

$$X = [A(1, :), A(2:m, n)] \tag{3}$$

where  $A(1,:)$  is the first row of matrix  $A$ , and  $A(2:m, n)$  is the last column without the first element. Through SVD method,  $A$  can be converted as

$$A = \sigma_1 u_1 v_1^T + \sigma_2 u_2 v_2^T + \cdots + \sigma_q u_q v_q^T \tag{4}$$

where  $\{u_i\}$  and  $\{v_i\}$  are column vectors of  $U$  and  $V$ .  $u_i \in R^{m \times 1}$ ,  $v_i \in R^{n \times 1}$  ( $i = 1, 2, \dots, q$ ), and  $u_i v_i^T \in R^{m \times n}$ . It is obvious that  $\sigma_i$  is actually the projection of matrix  $A$  on the basis  $u_i v_i^T$ . These  $\{\sigma_i\}$  ( $i = 1, 2, \dots, q$ ) are called singular values (SVs) of  $A$ .

**Step 3: Reconstruction.** Define  $A_i = \sigma_i u_i v_i^T$ , then

$$A = \sum_{i=1}^q A_i \tag{5}$$

The relationship between  $A_i$  and  $R_{i,1}$ ,  $C_{i,n}$  is shown in Fig. 1. A component signal  $P_i$  can be expressed as the vector form

$$P_i = [R_{i,1}, C_{i,n}^T]; \quad R_{i,1} \in R^{1 \times n}, \quad C_{i,n} \in R^{(m-1) \times 1} \tag{6}$$

From Eqs. (3), (5) and (6), the original signal equals the sum of component signals, which can be written as

$$X = \sum_{i=1}^q P_i \tag{7}$$

Sometimes the diagonal averaging is utilized for reconstruction [14,16]. When the component signals are used for the further feature extraction, the reconstruction method does matter a lot. But in this paper, the focus is on singular values. So the description of Step 3 is just for the completeness of knowledge expression.

**Step 4: Feature extraction.** A SV vector is obtained from Step 2, which can be shown as

$$SV = \{\sigma_1, \sigma_2, \dots, \sigma_q\} \tag{8}$$

where  $q = \min(m, n)$ .

The neighboring singular value ratio (NR) is proposed with the formulation

$$NR_i = \sigma_i / \sigma_{i+1} \tag{9}$$

Then a NSVR vector can be defined as

$$NSVR = \{NR_1, NR_2, \dots, NR_{q-1}\} \tag{10}$$

A bearing under different fault states has different frequency distributions, and component signals obtained by SVD have different frequency spectra. Then NSVR can be influenced according to the bearing fault condition. So NSVR vector is chosen as the feature representing the fault type. Until now SV feature vector and NSVR feature vector are extracted as

$$SV - NSVR = \{SV, NSVR\} \tag{11}$$

where SV-NSVR is a  $(2q - 1)$ -dimension vector.

### 3. Hidden Markov model

HMM is a dual random process which has hidden Markov chains with a given number of states and obvious random function set [20]. Each function is relevant to a state of the chains, and the hidden process cannot be observed. HMM has a

strong capability of pattern classification, especially for non-stationary signals. Recently, many research results have been reported on the application of HMM in the fault diagnosis. Ocak [35,36] introduced HMM into the bearing fault detection and diagnosis scheme. In reference [37], Ocak proposed the wavelet packet decomposition (WPD) and HMM based bearing fault tracking scheme. Bunks and McCarthy discussed how HMM could be applied to the problem of machine health monitoring, machine diagnostics and prognostics by comparing similarities of condition-based maintenance (CBM) to those of speech processing [38]. Li et al. proposed and verified that the HMM-based fault diagnosis approach for the speed-up and speed-down process was feasible and effective [39]. In reference [40], the average probability index (API) as a probabilistic health description index calculated based on HMM was proposed for gearbox health evaluation. Miao et al. [41] presented an on-line fault classification system with an adaptive model re-estimation algorithm. Because of the wide and successful applications in machinery fault diagnosis and health management, HMM is used for the automatic classification in this paper. And details of HMM are described in the following sections.

### 3.1. Elements of HMM

One hidden Markov model can be expressed by following parameters:

- (1)  $N$ : the number of states in the model. Suppose  $S_1, S_2, \dots, S_N$  are  $N$  states of the model, and  $q_t$  stands for the state the model stays at the moment  $t$ . Obviously,  $q_t \in \{S_1, S_2, \dots, S_N\}$ .
- (2)  $M$ : the number of distinct observation symbols per state. Suppose  $v_1, v_2, \dots, v_M$  are  $M$  distinct observations, and  $o_t$  stands for the observation at the moment  $t$ . Obviously,  $o_t \in \{v_1, v_2, \dots, v_M\}$ .
- (3)  $\pi$ : the initial state probability distribution.  $\pi = \{\pi_i\}$ , where  $\pi_i = P(q_1 = S_i)$ ,  $1 \leq i \leq N$ .
- (4)  $A$ : the state transition probability matrix.  $A = \{a_{ij}\}$ , where  $a_{ij} = P(q_{t+1} = S_j | q_t = S_i)$ ,  $1 \leq i, j \leq N$ .
- (5)  $B$ : the observation symbol probability matrix.  $B = \{b_j(k)\}$ , where  $b_j(k) = P(o_t = v_k | q_t = S_j)$ ,  $1 \leq j \leq N$ ,  $1 \leq k \leq M$ .

Based on the above introduction, one HMM can be described by  $N, M, \pi, A$  and  $B$ . For convenience, the notation  $\lambda = (\pi, A, B)$  is used to indicate the complete parameter set of the model.

### 3.2. Algorithms of HMM

There are three basic algorithms in HMM, namely the Forward–Backward procedure, Viterbi algorithm and Baum–Welch algorithm [20,41]. They are introduced respectively as follows:

- (1) Forward–Backward procedure: When a mode  $\lambda$  and a sequence of observations  $O = (o_1, o_2, \dots, o_T)$  are given, the probability that the observed sequence is generated by the model  $\lambda$  can be calculated.
- (2) Viterbi algorithm: When a mode  $\lambda$  and a sequence of observations  $O = (o_1, o_2, \dots, o_T)$  are given, an optimal state sequence  $Q = (q_1, q_2, \dots, q_T)$  can be obtained.
- (3) Baum–Welch algorithm: This algorithm is for HMM parameters re-estimation, outputting parameters  $\lambda = (\pi, A, B)$  to maximize the probability of the observation sequence.

The detailed Viterbi algorithm for HMM is given in Appendix A. Appendix B provides details on Forward–Backward algorithm for HMM. The parameter estimation for HMM can be found in Appendix C. In most cases, the signal analyzed is continuous. So the HMM discussed before is not appropriate. Continuous HMM (CHMM) is an extension of HMM for continuous signals and utilizes continuous observation densities. Usually, a Gaussian mixture model (GMM) is adopted to ensure the observation probability of the model [42] as

$$b_j(o_t) = \sum_{m=1}^{M_j} w_{j,m} b_{j,m}(o_t) = \sum_{m=1}^{M_j} w_{j,m} N(o_t, \mu_{j,m}, \Sigma_{j,m}) \quad (12)$$

where  $M_j$  is the number of Gaussian mixtures in the state  $S_j$ , and  $w_{j,m}$  is the mixture weight of the  $m$ 'th Gaussian mixture in the state  $S_j$ .  $N(\cdot)$  defines a Gaussian density with a mean vector  $\mu_{j,m}$  and a covariance matrix  $\Sigma_{j,m}$  for the  $m$ 'th Gaussian mixture in the state  $S_j$ . In this paper, the data sampled is discrete value of continuous time series, therefore it is advantageous to utilize CHMM.

## 4. Bearing fault diagnosis and performance assessment based on SV–NSVR and CHMM

As CHMM is applied for the fault diagnosis and performance assessment, the process consists of two procedures: training and testing. There are two experiments in this work. One is the bearing fault diagnosis using SV–NSVR and CHMM; another is the bearing performance assessment based on SV–NSVR and CHMM. There are some differences for CHMM procedures between these two applications. The detailed procedures of these two applications are introduced in the following sections.

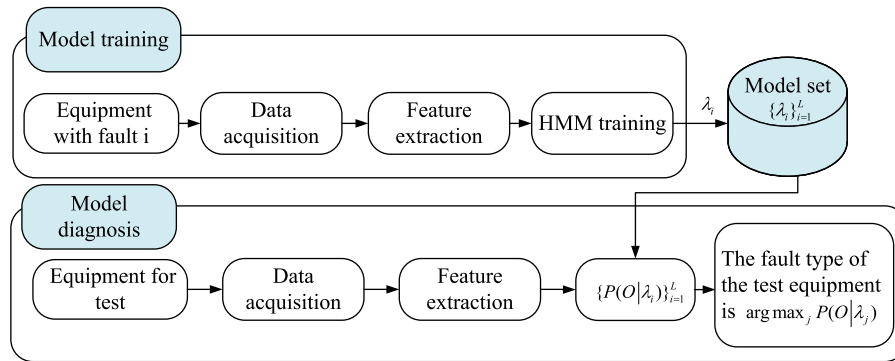


Fig. 2. The SV-NSVR and CHMM based fault diagnosis scheme.

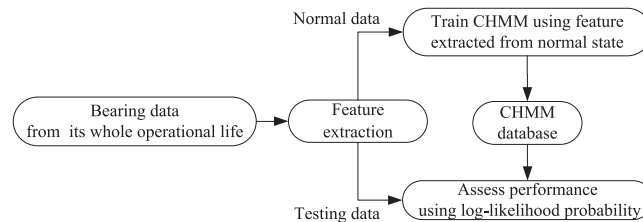


Fig. 3. The scheme of bearing performance assessment.

#### 4.1. Bearing fault diagnosis based on SV-NSVR and CHMM

**Training procedure:** All types of typical faults in rolling element bearings are properly sampled and preprocessed. Then, their feature vectors are extracted using the SV-NSVR feature extraction method introduced in Section 2. These sets of SV-NSVR vectors are taken as observation sequences and input into CHMM of each fault mode for training using the Baum-Welch algorithm in Section 3. **Testing procedure:** Once the CHMM model set of each fault mode is established, the bearing fault diagnosis can be realized. Then the procedure of the bearing fault diagnosis based on CHMM is as follows: given a sequence of observations (SV-NSVR vectors calculated from sample data), the probability of each mode is calculated. And the CHMM with the maximum probability determines the condition of the testing data. The probability of the observation sequence can be calculated using the Forward-Backward algorithm in Section 3. Fig. 2 illustrates the scheme of SV-NSVR and CHMM based fault diagnosis, where  $L$  is the number of fault types.

#### 4.2. Bearing performance assessment based on SV-NSVR and CHMM

Recently, performance degradation assessment, the base of prognosis which is more efficient than the fault diagnosis to realize condition-based maintenance, has been proposed and received more and more attention [5,43–45]. In order to verify the effectiveness of the presented feature extraction method, the SV-NSVR and CHMM based performance assessment is implemented in the experiment 2. When applying CHMM to the bearing performance assessment, procedures are kind of different from the fault diagnosis. The main scheme is shown in Fig. 3. **For the training procedure**, the method is the same with the diagnosis scheme. However, only one CHMM is trained using sample data from the bearing under normal condition. After CHMM is established, the performance assessment work can be carried on. **For the testing procedure**, the online sample data (after feature extraction) is put into the CHMM to assess the current condition of the testing bearing. When the testing bearing is degraded, the condition of bearing is different from normal condition, which leads to the output of CHMM decreasing. So the output probability of CHMM can be treated as the performance index (PI) to assess the bearing performance. After some threshold values are predetermined, the CHMM-based performance assessment system can monitor the bearing condition intelligently. To increase the reliability of PI and reduce the number of false alarms when threshold values are set, the probability output from CHMM is processed with exponential weight moving average technique.

In the following sections, two experiments will be introduced to display the validity of SV-NSVR and CHMM based method for the bearing fault diagnosis and performance assessment.

### 5. Experiment 1: artificial fault diagnosis of rolling element bearings

The SV-NSVRs are the representation of the signal in the singular spectrum domain. At the end of Step 4 of the SV-NSVR feature extraction method in section 2,  $(2q-1)$ -dimension (where  $q = \min(m, n)$ ) SV-NSVR feature vectors are obtained.

SV–NSVR representations of fault conditions are influenced by the window length  $m$ . So SV–NSVR features for different bearing conditions are compared and then the appropriate  $m$  and SV–NSVRs are selected. They are adopted as inputs to CHMM for the training and diagnosis. This method is tested with the vibration signal of the experiment 1, which is described in the subsequent sections.

### 5.1. Experiment introduction

To validate the proposed bearing fault diagnosis method, an artificial fault experiment was carried out. The test rig is shown in Fig. 4(a). The shaft of the machine was driven by an a.c. motor through a rub belt and a shaft coupling, and supported by a rotor back-up device. The testing bearing was fitted on the shaft. Its outer race was fixed by a fixture and its inner race rotated with the shaft. The rotating speed of the shaft was 720 r/min. A data acquisition (DAQ) system was installed to measure the bearing vibration. In the DAQ system, a bracket was introduced and stuck on the testing bearing. An accelerometer (Kistler 8791A250) was attached on the bracket by an adhesive mounting. The location of the accelerometer is shown in Fig. 4(b). The vibration signal picked up by the accelerometer was amplified through a charge amplifier (Kistler 5134A). Then, the output was fed to an NI PXI system (an NI PXI-1042 chassis with NI PXI-4472 modules). Finally, acquired signals were recorded by a computer installed with the DAQ software coded in NI LabVIEW. The sampling rate was 25.6 kHz.

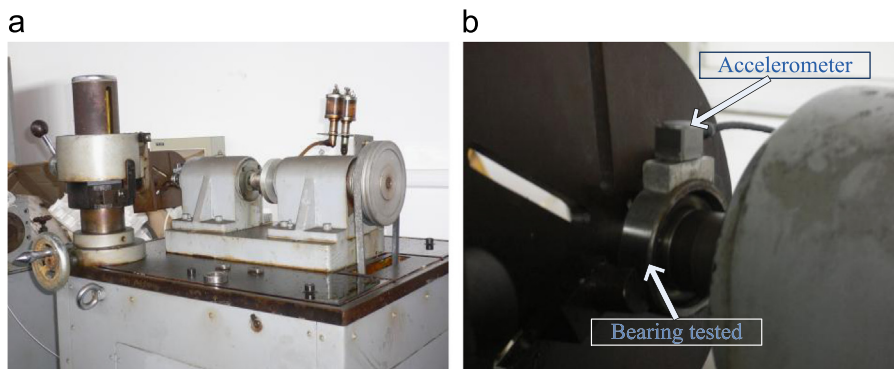


Fig. 4. (a) The rolling element bearing test rig and (b) the location of the accelerometer.

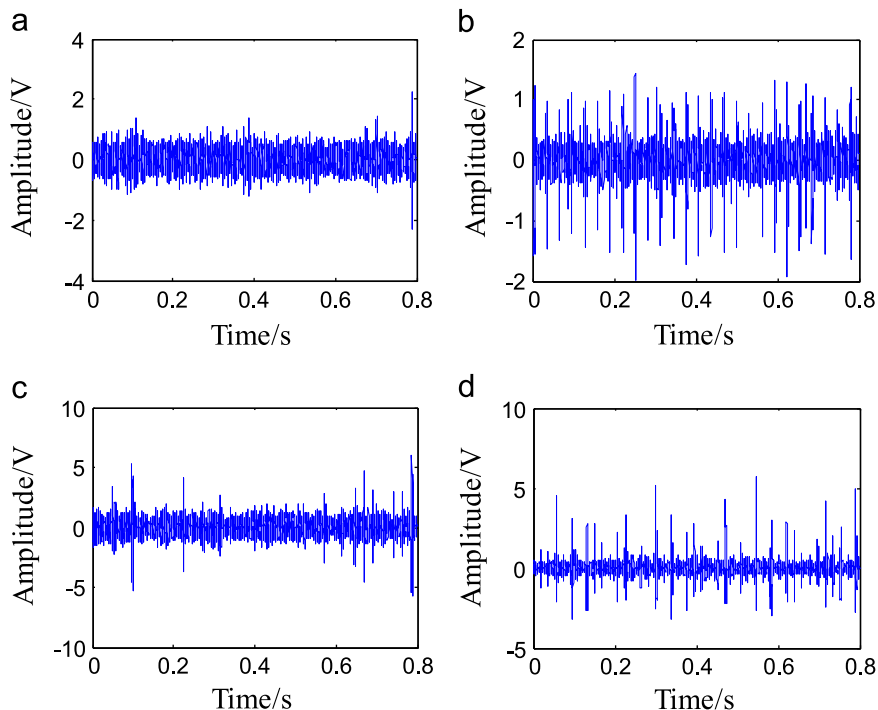


Fig. 5. Vibration signals from four rolling element bearings: (a) the normal bearing; (b) the bearing with outer race fault; (c) the bearing with rolling body fault; and (d) the bearing with inner race fault.

A series of GB203 rolling element bearings were used as testing bearings in this experiment. Single pitting faults were introduced to the surface of the race or the rolling body of the testing bearing by electrical-discharge machining method. The duration of each sample was 0.8 s. In this experiment, four bearing conditions are analyzed, which include normal condition (NC), inner race fault (IRF), outer race fault (ORF) and rolling body fault (RBF). Fig. 5 shows raw vibration signals of rolling element bearings under four different conditions.

5.2. Test data analysis

5.2.1. Selection of SV-NSVRs

**Choice of window length:** Different window lengths ( $2 \leq m \leq 9$ ) are used for embedding the signal, and corresponding  $m$ -dimension SVs are obtained based on the procedure as given in Section 2. These SVs are plotted with respect to their numbers and normalized using the min–max normalization technique. The normalized SV plots of bearing vibration signals in healthy and fault conditions for values of  $2 \leq m \leq 9$  are shown in Fig. 6. The larger SV in the singular spectrum represents the larger amplitude component in the decomposition, and the low-amplitude components of the signal are represented by the smaller SVs. In order to obtain more SVs, a bigger window length should be selected. However, as shown in Fig. 6, some SVs are already smaller than 0.01 when the window length is 9. When  $m$  takes bigger values, more small SVs are obtained. The SVs smaller than 0.01 represent spectrum components which can be ignored. So the window length of 9 is selected representing a good compromise between the quantity and the quality of SV features. For instance, one sample data from the bearing with outer race fault is chosen to display the results of Hankel matrix-based SVD when the window length is 9. The time wave and the spectrum of original signal are shown in Fig. 7(a) and (b). The time waves and spectra of nine component signals obtained by Hankel matrix-based SVD are shown in Fig. 7(c) and (d). It can be seen from Fig. 7 that (1) in (d), the peak of

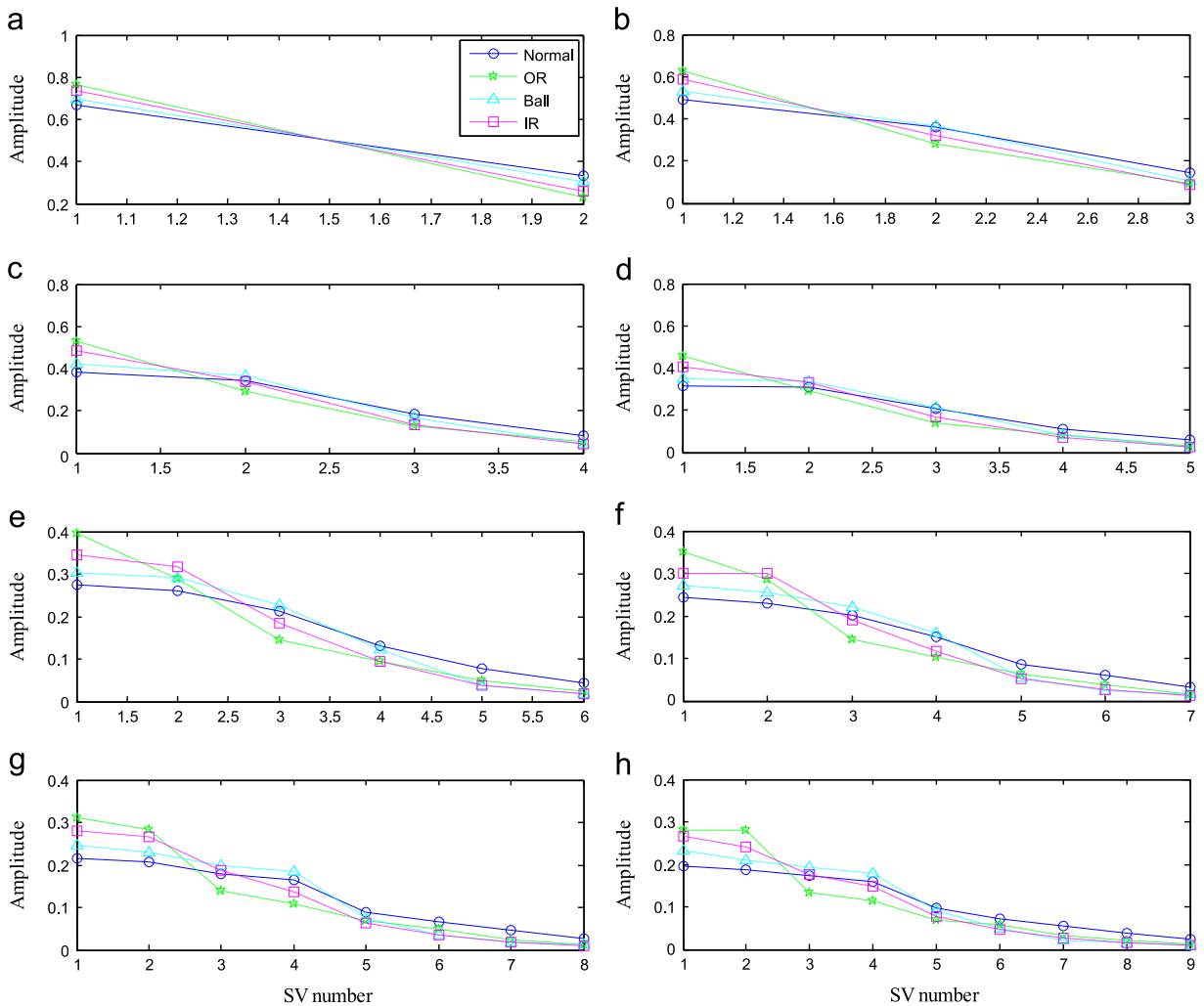


Fig. 6. The normalized singular values obtained by Hankel matrix-based SVD: (a)–(h) results for  $2 \leq m \leq 9$ .

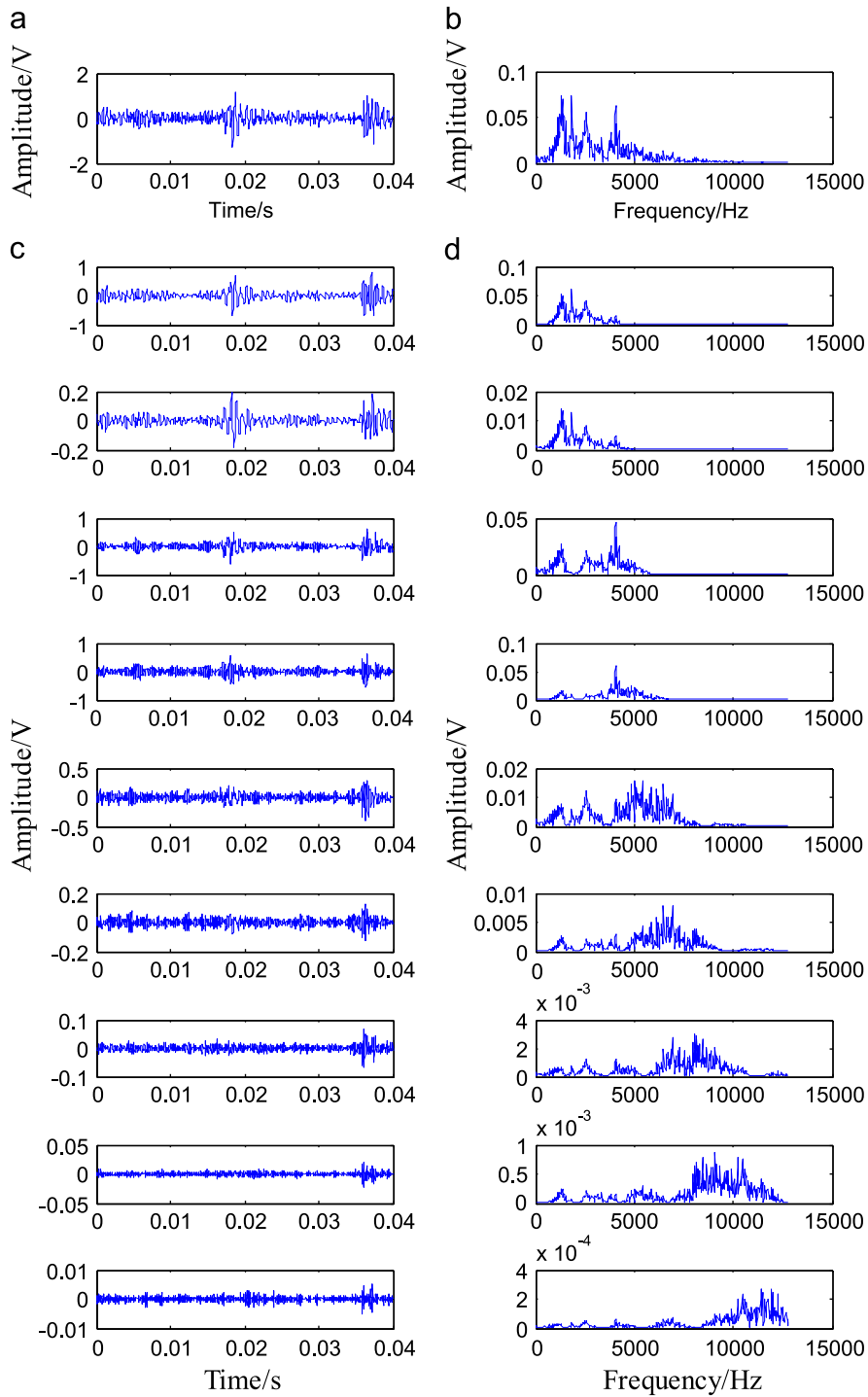


Fig. 7. (a and b) The time wave and spectrum of original signal and (c and d) the time waves and spectra of component signals.

spectrum is moving to high frequency domain slowly and (2) the spectrum of each component distributes in different frequency domain, which means the components represent different spectral components.

**Selection criteria of SV-NSVRs:** When the window length is 9, an example of SVs and NSVRs obtained by Hankel matrix-based SVD is shown in Fig. 8. The SV-NSVR feature vector extracted is 17-dimension. It is not suitable for calculation. Usually, 5–10 parameters are enough from the view of calculation time and accuracy. In order to solve this problem, a new parameter evaluation technique to select features was proposed by Yang [46] and improved by Lei [47,48]. The improved

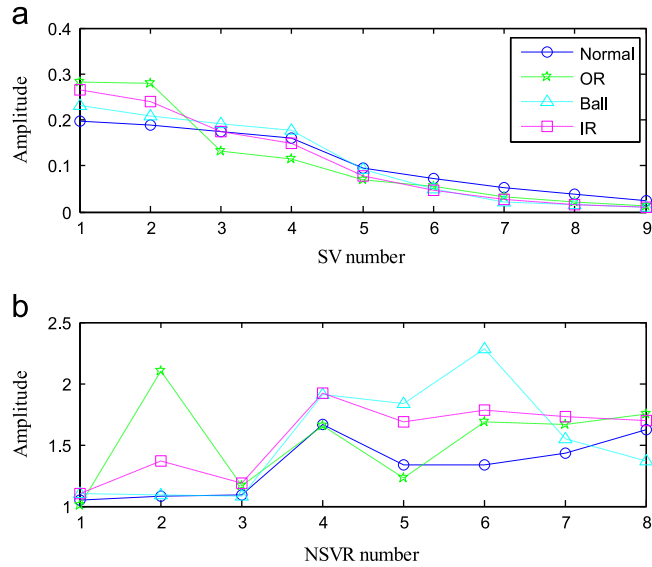


Fig. 8. SVD results of the original signal when the window length is 9: (a) SVs and (b) NSVRs.

technique has better performance for feature weighting problem. The algorithm of the feature evaluation is described as follows:

Suppose the feature set under  $C$  kinds of fault states ( $\omega_1, \omega_2, \dots, \omega_c$ ) is defined as

$$\{p_{c,m,k}, \quad c = 1, 2, \dots, C; \quad m = 1, 2, \dots, M_c; \quad k = 1, 2, \dots, K\} \tag{13}$$

where  $p_{c,m,k}$  is the  $k$ 'th feature of sample  $m$  when the fault state is  $\omega_c$ .  $M_c$  is the number of samples under the fault state  $\omega_c$ .  $K$  is the dimension of the feature.

Step 1: Calculate the average distance between each feature under the fault state  $\omega_c$

$$d_{c,k} = 1/(M_c \times (M_c - 1)) \sum_{i=1}^{M_c} \sum_{j=1}^{M_c} |p_{c,i,k} - p_{c,j,k}| \tag{14}$$

For  $c=1, 2, \dots, C$ , the average distance under the same fault state is calculated as

$$d_k^w = 1/C \sum_{c=1}^C d_{c,k} \tag{15}$$

Step 2: Calculate the average distance among  $C$  kinds of fault states for each feature

$$d_k^b = 1/(C \times (C - 1)) \sum_{c=1}^C \sum_{e=1}^C |\mu_{e,k} - \mu_{c,k}| \tag{16}$$

where  $\mu_{c,k} = 1/M_c \sum_{m=1}^{M_c} p_{c,m,k}$ , and it is the mean of the  $k$ 'th feature under the fault state  $\omega_c$ .

Step 3: Calculate the ratio  $d_k^b/d_k^w$  as the assessment indicator of  $k$ 'th feature

$$J_k = d_k^b/d_k^w \tag{17}$$

Normalize  $J_k$

$$\bar{J}_k = J_k / \max(J_k) \tag{18}$$

$\bar{J}_k$  is the effectiveness factor of the  $k$ 'th feature. The effectiveness factors of the 17-dimension SV–NSVR feature are shown in Fig. 9. Features with effectiveness factor higher than 0.7 are selected. Then selected features are  $\sigma_5, \sigma_7, \sigma_8, \sigma_9, \sigma_5/\sigma_6$  and  $\sigma_6/\sigma_7$ . These features are then used as inputs to CHMM for training and diagnosis. Based on the output of CHMM, the testing bearings are diagnosed.

5.2.2. Bearing fault diagnosis based on CHMM

The selected SV-NSVRs are utilized as inputs of CHMM for bearing fault diagnosis. 200 feature datasets are extracted for each bearing condition. And 150 of these feature datasets are selected randomly as observation sequences for training. Then the other 50 datasets are taken as testing data. As introduced in Section 5.1, there are four types of bearing fault conditions being tested, which are normal condition (NC), inner race fault (IRF), outer race fault (ORF) and rolling body fault (RBF). Four CHMMs (one CHMM for each bearing condition) need to be trained. The CHMMs with four states, each state with two Gaussian mixtures, are trained using the selected feature databases. The initialization and estimation of CHMM parameters are achieved through the parameters estimation algorithm presented in Appendix C respectively for each bearing condition.

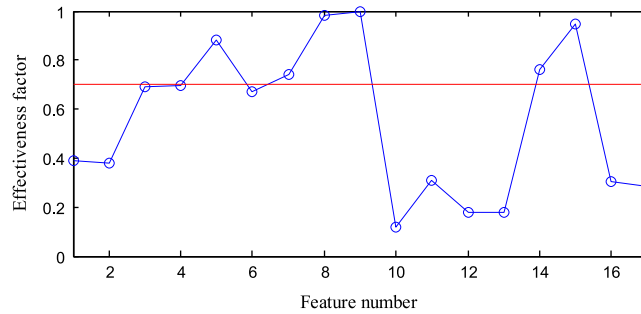


Fig. 9. The effectiveness factors of the SV-NSVR features.

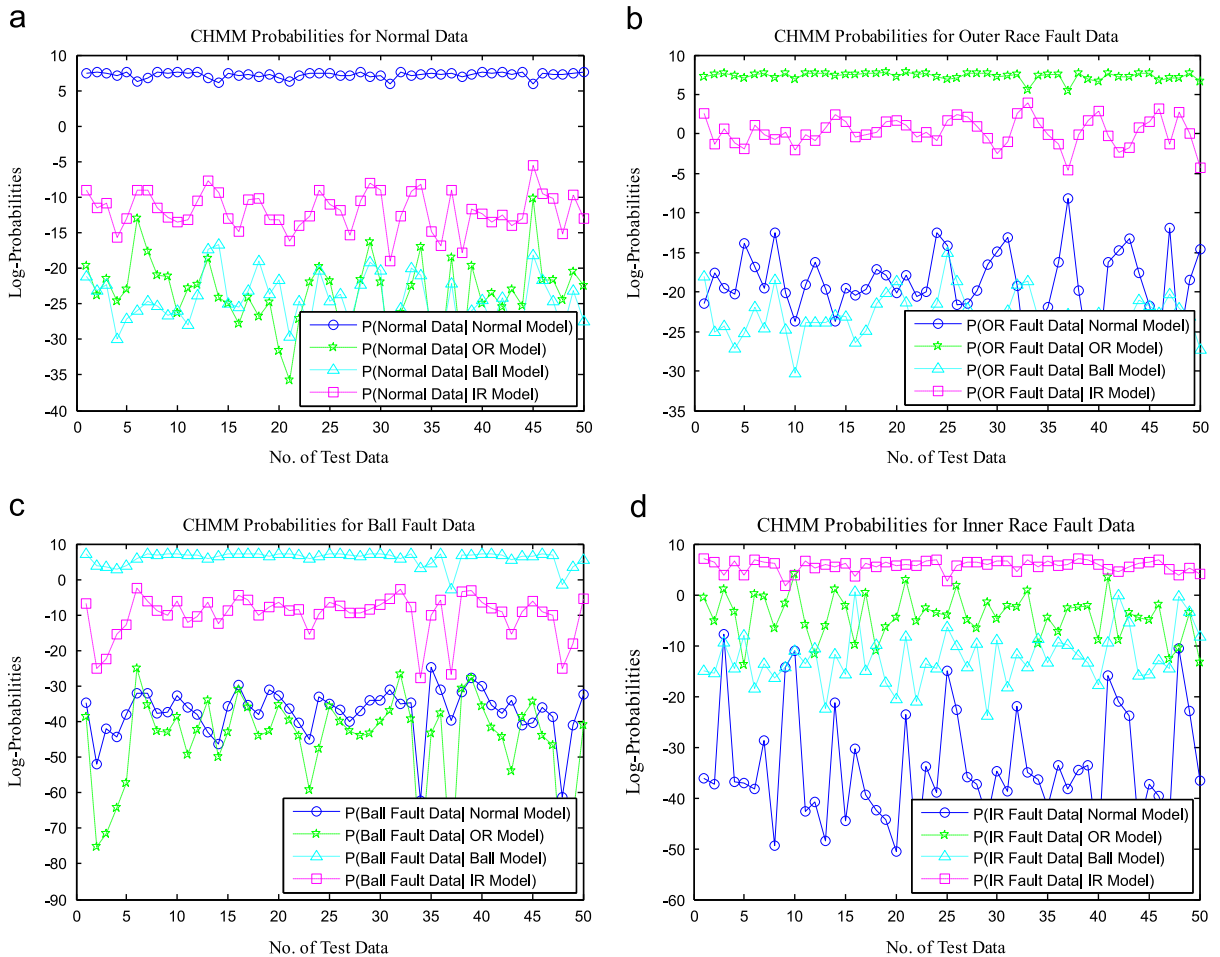


Fig. 10. Results using selected SV-NSVRs and CHMM for bearing fault diagnosis: (a) CHMM probabilities under four CHMM models for normal data; (b) CHMM probabilities under four CHMM models for outer race fault data; (c) CHMM probabilities under four CHMM models for rolling body fault data; and (d) CHMM probabilities under four CHMM models for inner race fault data.

Hereto, four CHMMs are obtained which are  $\lambda_{NC}$ ,  $\lambda_{ORF}$ ,  $\lambda_{RBF}$  and  $\lambda_{IRF}$ . Then the testing feature databases can be input into these CHMMs for classification.

Fig. 10 provides diagnosis results for the NC testing data, the ORF testing data, the RBF testing data and the IRF testing data, respectively. As shown in Fig. 10(a), distances between outputs of the NC model and the other models are quite obvious. All normal samples are diagnosed correctly. The diagnosis results of ORF testing samples are shown in Fig. 10(b). Although distances between outputs of the ORF model and the other CHMMs are smaller, all ORF samples get the highest values from  $\lambda_{ORF}$  compared with those from all the other pre-trained CHMMs. The same situation occurs for the IRF testing data which is shown in Fig. 10(c). Testing samples are ordered from 1 to 50. For the IRF testing data, distances between outputs of four CHMMs are much smaller. However, separations of outputs from four CHMMs are still obvious as shown in Fig. 10(d). So the diagnosis of IRF is successful except that the No. 10 IRF sample is diagnosed as ORF mistakenly. It can be concluded that the selected SV–NSVR and CHMM based method is quite effective for the bearing fault diagnosis.

5.2.3. Comparisons with other SVD features

In many applications, SVs are chosen as features for the fault diagnosis [16,30]. For the validation of the proposed feature extraction method, other same dimensional features obtained by SVD are selected for the bearing fault diagnosis. On one hand, 6-dimension SVs are selected as feature databases for CHMM-based bearing fault diagnosis to validate the significance of the NSVR; on the other hand, 6-dimension NSVRs are chosen as features to prove that SVs and NSVRs are complementary to each other for the representation of the bearing fault information. Based on the parameter evaluation technique mentioned in Section 5.2.1, six SVs with the highest effectiveness factors are selected, which are  $\sigma_3$ ,  $\sigma_4$ ,  $\sigma_5$ ,  $\sigma_7$ ,  $\sigma_8$  and  $\sigma_9$ . And  $\sigma_2/\sigma_3$ ,  $\sigma_3/\sigma_4$ ,  $\sigma_5/\sigma_6$ ,  $\sigma_6/\sigma_7$ ,  $\sigma_7/\sigma_8$  and  $\sigma_8/\sigma_9$  are the selected NSVRs. Then diagnosis results based on SVs–CHMM and NSVRs–CHMM are respectively shown in Figs. 11 and 12.

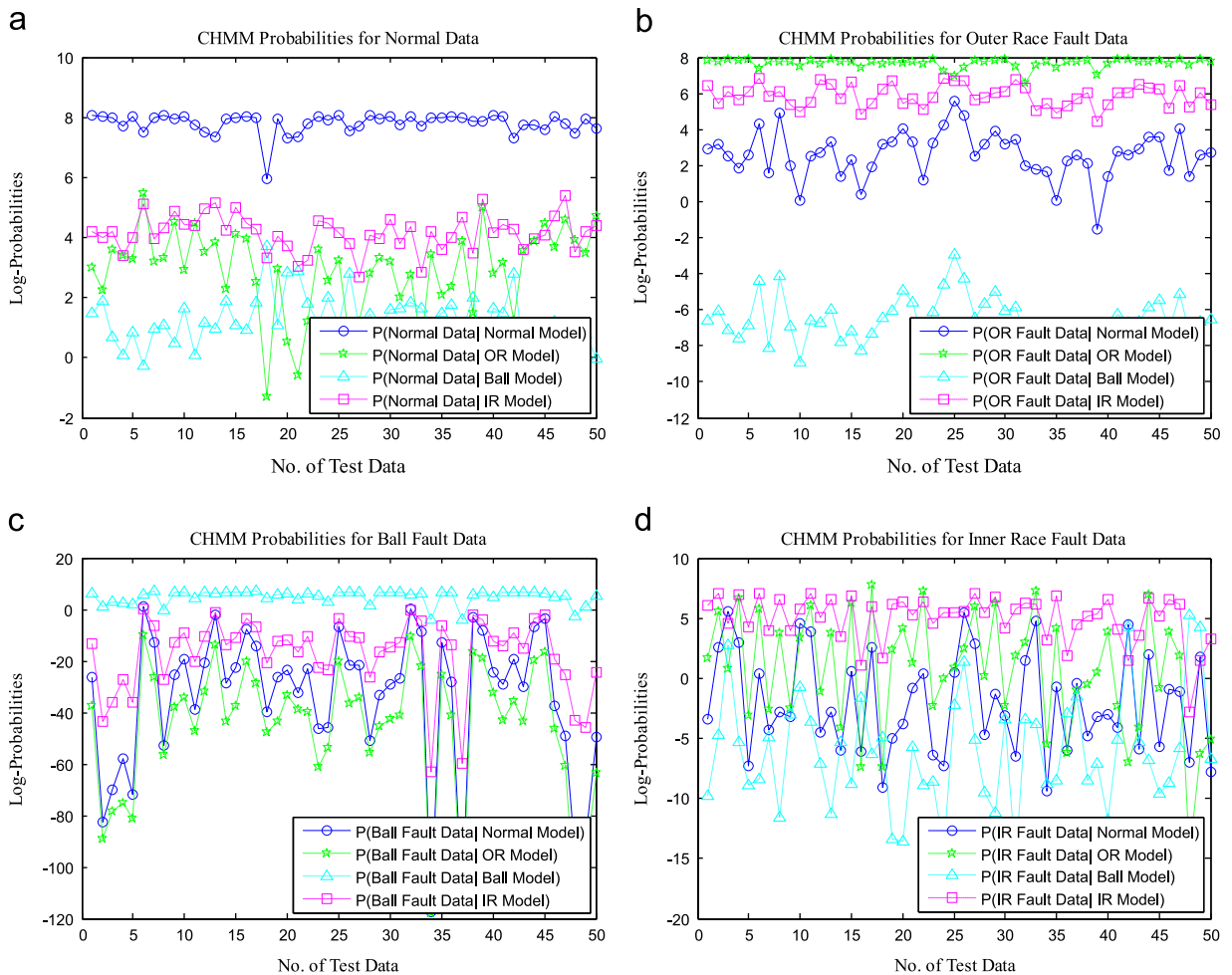
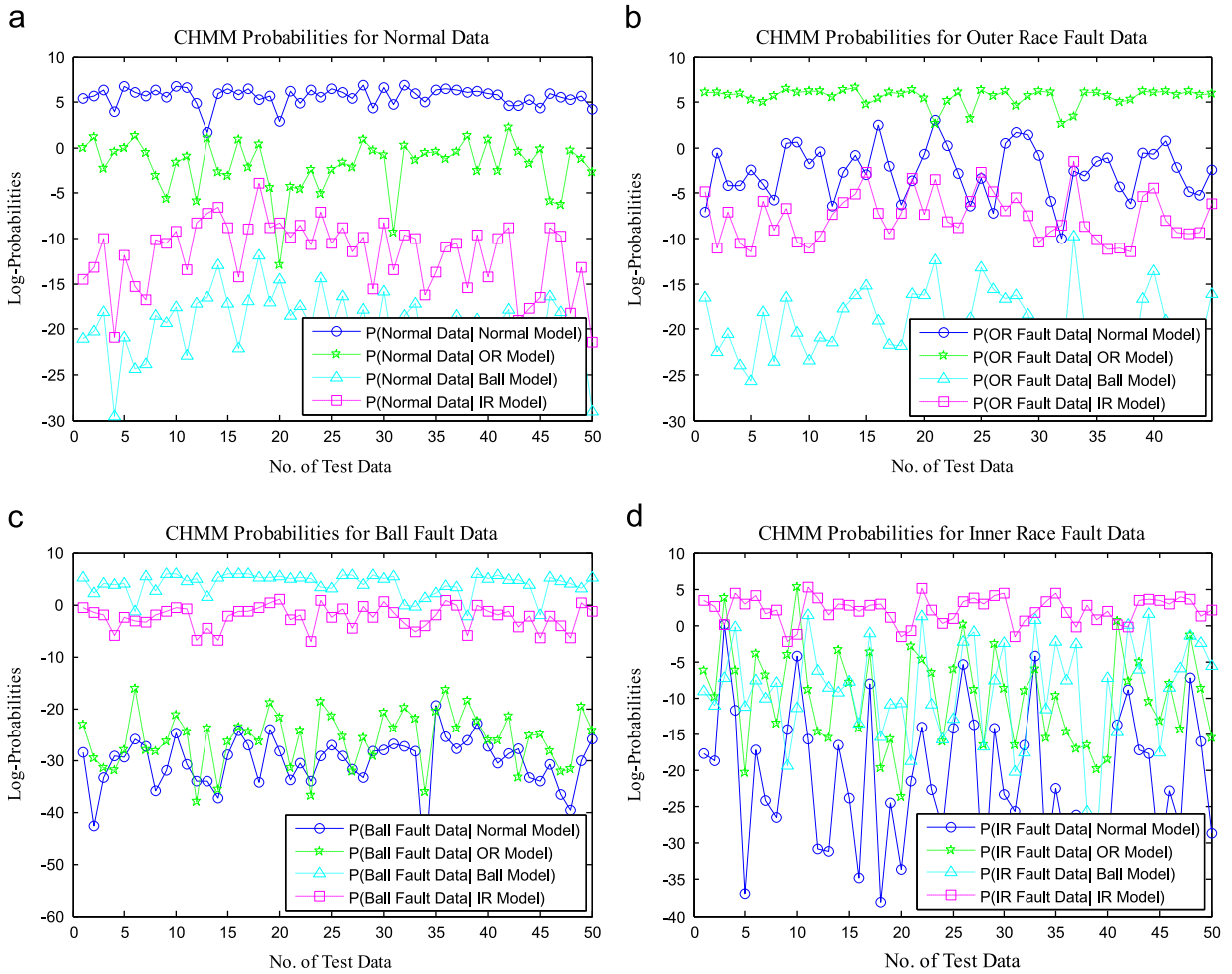


Fig. 11. Results using the top 6 SVs and CHMM for bearing fault diagnosis: (a) CHMM probabilities under four CHMM models for normal data; (b) CHMM probabilities under four CHMM models for outer race fault data; (c) CHMM probabilities under four CHMM models for rolling body fault data; and (d) CHMM probabilities under four CHMM models for inner race fault data.



**Fig. 12.** Results using the top 6 NSVRs and CHMM for bearing fault diagnosis: (a) CHMM probabilities under four CHMM models for normal data; (b) CHMM probabilities under four CHMM models for outer race fault data; (c) CHMM probabilities under four CHMM models for rolling body fault data; and (d) CHMM probabilities under four CHMM models for inner race fault data.

For the NC bearing diagnosis: both SVs–CHMM and NSVRs–CHMM method can diagnose the NC data successfully. However, distances between outputs of the NC CHMM and the other CHMMs are much smaller especially for the NSVRs–CHMM based method. For the ORF bearing diagnosis: the SVs–CHMM based method can barely diagnose all the testing data correctly. Although distances between outputs of the ORF CHMM and the other CHMMs are much bigger for the NSVRs–CHMM based method, the No. 21 ORF sample is diagnosed as NC mistakenly. The results of the RBF bearing diagnosis are similarly to those of the NC bearing diagnosis. For the IRF bearing diagnosis: as shown in Fig. 11(d), eight IRF samples are diagnosed wrong (No. 3 and 42 samples are diagnosed as NC; Nos. 17, 22, 33 and 44 samples are recognized as ORF; Nos. 48 and 49 samples are classified as RBF); as depicted in Fig. 12(d), four IRF samples are diagnosed wrong (Nos. 3, 10 and 41 samples are recognized as ORF; No. 42 sample is diagnosed as RBF). From the above results, it is easy to know that (1) both SVs and NSVRs are less effective than SV–NSVRs for the representation of the bearing fault characteristic; (2) SVs and NSVRs have different performance in the CHMM-based bearing fault diagnosis (such as the NC and IRF bearing diagnosis).

The diagnosis accuracies of above methods are summarized in Table 1. The results show that the NSVR feature extraction is effective. Besides, the same dimensional SV–NSVR feature performs better in the CHMM-based bearing fault diagnosis compared with SVs and NSVRs.

## 6. Experiment 2: accelerated life test of rolling element bearings

### 6.1. Experiment introduction

The experiment discussed in Section 5 is a traditional method to study fault diagnosis using an artificial defect machining method. So it cannot simulate the state of natural fault in practice, especially when the incipient fault occurs. In order to

obtain the signal of natural fault, an accelerated life test was performed to acquire the signal of bearings over a whole lifetime.

The accelerated bearing life tester (ABLT-1A) was provided by Hangzhou Bearing Test & Research Center (HBRC), as shown in Fig. 13. The tester included an AC motor, a transmission system, a lubrication system, a loading system and a data acquisition system. It could install four bearings one time. In the test, a load of 12.744 kN was appended on bearings to accelerate bearings to failure. Three PCB348A acceleration sensors were included in the data acquisition system. The type of

**Table 1**  
Diagnosis results by different features.

Feature	Normal	Outer race fault	Rolling body fault	Inner race fault	Accuracy (%)
Top 6 SVs	50 (50)	50 (50)	50 (50)	42 (50)	96
Top 6 NSVRs	50 (50)	49 (50)	50 (50)	46 (50)	97.5
6 SV-NSVRs	50 (50)	50 (50)	50 (50)	49 (50)	99.5

Each testing database has 50 samples for each fault condition; the value out of the bracket is the number of samples diagnosed correctly.

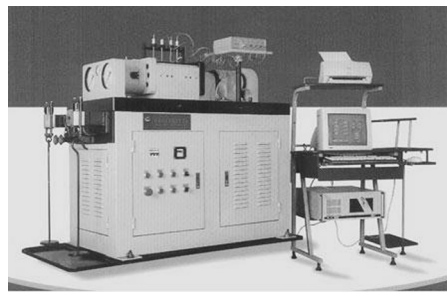


**Fig. 13.** Accelerated bearing life tester (ABLT-1A).

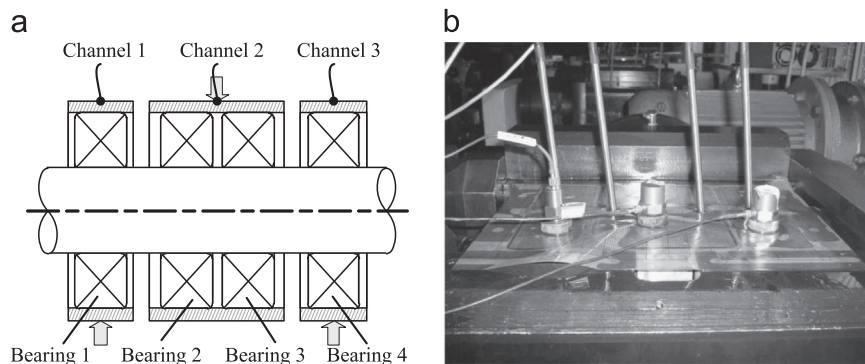


**Fig. 14.** Sketch of load and location of sensors: (a) sketch of load and (b) location of sensors.

**Table 2**  
Rolling element bearing parameters and operation conditions.

Type	Ball number	Ball diameter (mm)	Pitch diameter (mm)	Contact angle	Motor speed (rpm)	Load (kN)
6307	8	13.494	58.5	0	3000	12.744

**Table 3**  
Five characteristic frequencies of rolling element bearing 6307 (Hz).

$f_r$	$f_c$	$f_b$	$f_i$	$f_o$
50	19	102	246	153

data acquisition card was NI PCI-6023E. The sketch of load and the location of sensors are shown in Fig. 14. The data sampling rate was 25.6 kHz. 20,480 points were acquired per minute. The type of the testing bearing was 6307 and its corresponding parameters and operation conditions are displayed in Table 2. Five characteristic frequencies are shown in Table 3.

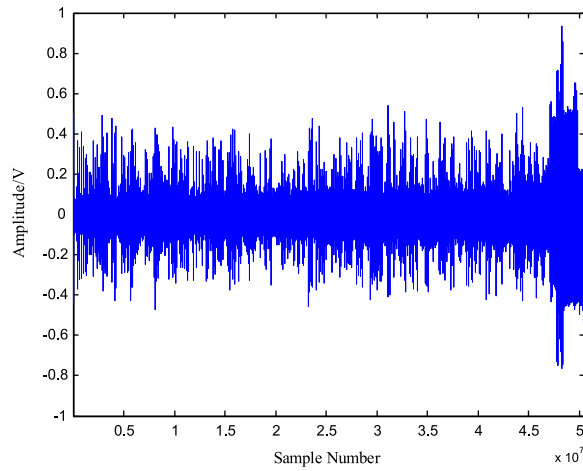


Fig. 15. Raw signal of the whole lifetime.

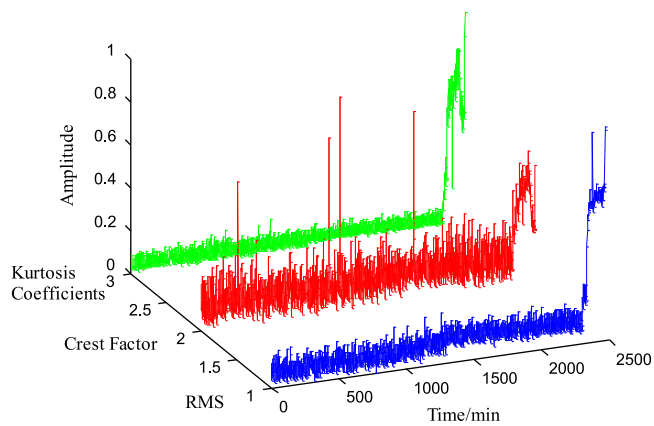


Fig. 16. Three frequently-used time domain features in the whole lifetime.

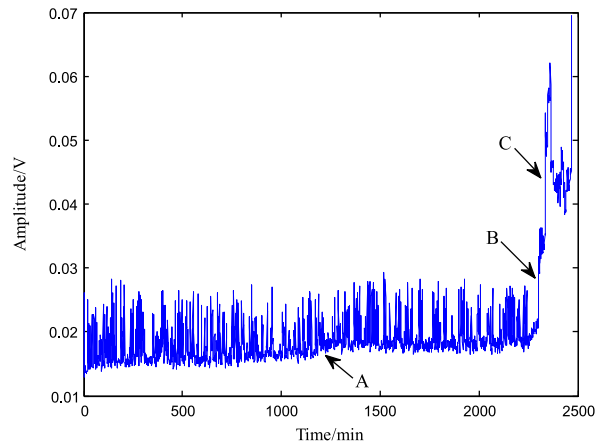


Fig. 17. Root mean square of bearing in the whole lifetime.

## 6.2. Bearing performance assessment based on SV-NSVR and CHMM

### 6.2.1. Original data analysis

The whole lifetime data were collected, as the bearing degenerated from normal condition to final failure. The total acquisition duration was 2469 min. The whole lifetime signal and three frequently-used time domain features are plotted in Figs. 15 and 16. The trends of the three features are similar. In order to show the degradation trend of the bearing during the whole lifetime more clearly, the root mean square (RMS) index is plotted separately in Fig. 17. Three obvious change moments can be recognized roughly which are donated as A, B and C as shown in Fig. 17. Except these three moments, the RMS curve fluctuates greatly during the whole lifetime. When a fault occurs, the vibration amplitude of the testing bearing will increase. So it can be inferred that the beginning 1000 min are under normal condition from the whole lifetime RMS.

### 6.2.2. Performance assessment

The details of the bearing performance assessment based on SV-NSVR and CHMM are illustrated in Section 4. One normal condition CHMM needs to be pre-trained. From the analysis in Section 6.2.1, the beginning 500 min databases are utilized for the normal condition CHMM establishment.

**Feature extraction:** The proposed SV-NSVRs are extracted as features. In Section 5.2.1, six features are selected for diagnosis. The selected features are sensitive to bearing faults which also meet the requirement of the CHMM-based performance assessment. These six features are extracted and compared with RMS curve as shown in Fig. 18. It can be found

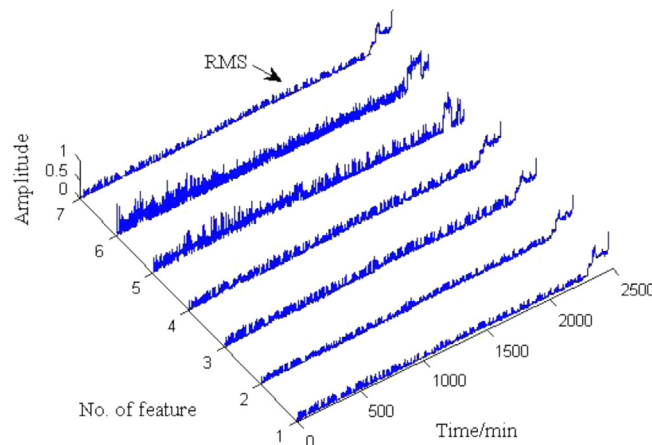


Fig. 18. The selected features and RMS in whole lifetime.

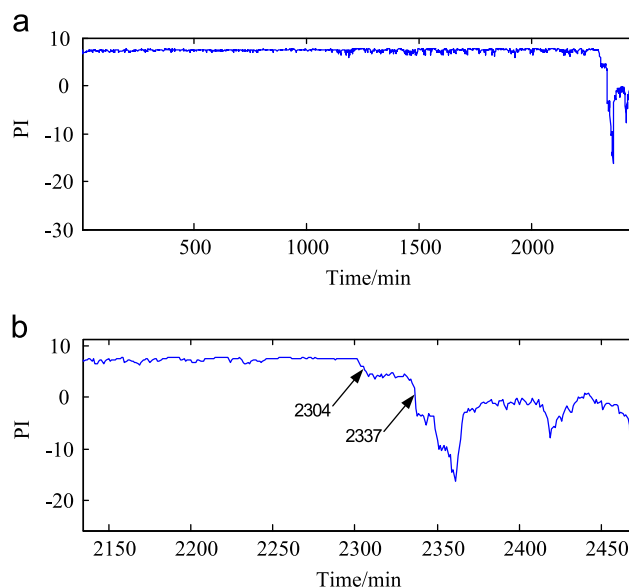


Fig. 19. (a) The performance index of bearing using selected SV-NSVR features and (b) local enlargement of part B in (a).

that the whole lifetime trends of the selected features and RMS are similar. The selected features change along with the testing bearing from normal condition to final failure. The selected SV–NSVRs can be treated as inputs to CHMM for model training and performance assessment.

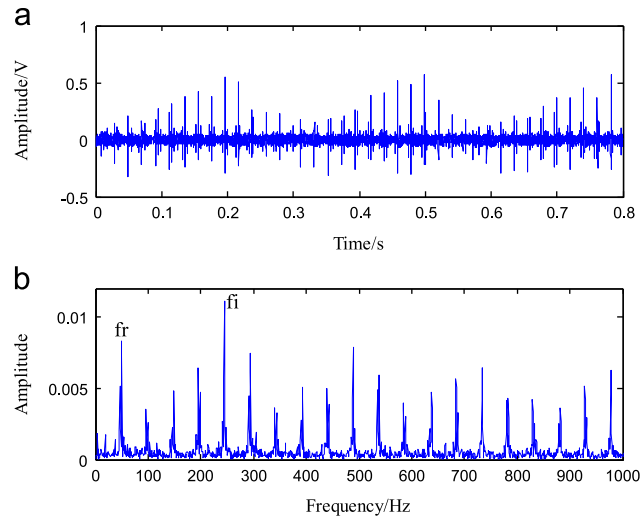


Fig. 20. (a) The original signal at 2304 min and (b) envelope spectrum.

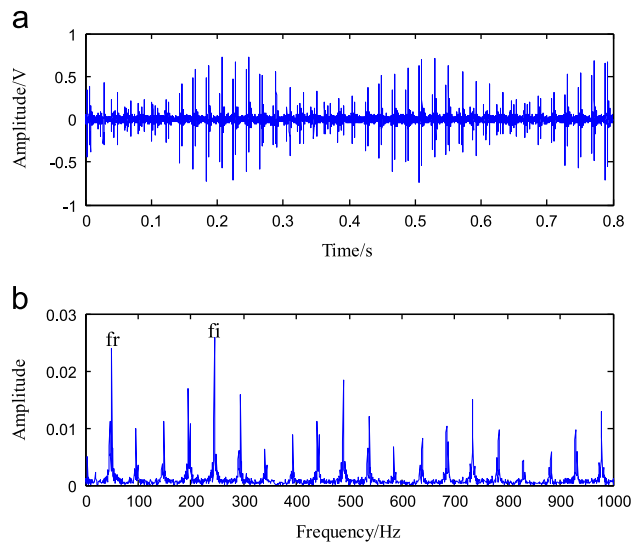


Fig. 21. (a) The original signal at 2337 min and (b) envelope spectrum.



Fig. 22. Bearing failure type.

**CHMM training and testing:** After feature extraction, the beginning 500 min feature databases are utilized for the normal condition CHMM training. Then the whole lifetime SV–NSVR feature database is put into the pre-trained CHMM to calculate the performance index. The assessment result is shown in Fig. 19.

From Fig. 19(a), it can be seen that the PI curve has two parts similar to RMS which cannot be neglected. (1) Fluctuations occur since the moment A, which is at around 1295 min; (2) in the part B, there are some obvious changes and the PI decreases quickly. It can be inferred that the degradation begins from the moment A. And the fault occurs and develops in part B. Early fault detection is meaningful for the condition monitoring and the enhancement of the fault development is the key of the performance assessment. So the local enlargement of part B is taken as shown in Fig. 19(b). The first significant decrease appears at 2304 min. Fluctuations keep for a few minutes. A bigger decrease occurs at 2337 min. Then the PI decreases quickly followed with a short time increase. At last, the PI decreases to failure.

From the above analysis, the moment 2304 min and 2337 min are two obvious change points for bearing early fault detection. The fault may occur at 2304 min and develop to severer level at 2337 min. The components which often fail in a rolling element bearing are the outer race, the inner race, the rolling body and the cage. Such failures generate a series of impact vibrations in short time intervals, which occur at bearing characteristic frequencies (BCF). Envelope analysis is always used with FFT to identify faults occurring at the BCF [49]. The time waves and envelope spectra of 2304 min and 2337 min are shown in Figs. 20 and 21 respectively. From Fig. 20, it can be seen that the time wave has a little fault characteristic. And the envelope spectrum covers the  $f_i$  (ball pass frequency inner race, BPFI) component, which is accompanied by the rotating speed frequency. In Fig. 21, the impulse is more obvious and the amplitude is higher, which means the fault degree is severer. A conclusion can be made that the IRF characteristic is obvious. And the failure type of the testing bearing is indeed inner race fault which is shown in Fig. 22. So the PI curve reflects the bearing performance degradation process effectively.

**Comparison and conclusion:** Comparing Figs. 17 and 19, the RMS and PI values both can describe the trend of the performance. Before 2304 min, the bearing may be normal or with quite weak fault which is not obvious. But since 2304 min, the vibration is becoming bigger and bigger and it may cause defects on the other components of the equipment. Furthermore, after 2337 min the bearing is running to failure along with serious consequences. In order to avoid the damage of other components and the heavy losses of industrial production, the alarm at 2304 min is very important. However, the RMS curve has big fluctuations which may cause false alarms when the threshold value is pre-set. The alarm at 2304 min is quite helpful for equipment maintenance. And the change at 2304 min is quite obvious and recognizable in the PI curve. So the selected SV–NSVR and CHMM based bearing performance assessment method is more effective.

## 7. Conclusions

In this study, a feature extraction method called SV–NSVR is proposed based on Hankel matrix-based SVD. After feature selection, the selected SV–NSVRs and CHMM are applied to the rolling element bearing fault diagnosis. In the artificial rolling bearing fault experiment, the detailed process of applying the selected SV–NSVRs and CHMM based method to bearing fault diagnosis is described. By comparing the diagnosis results of the proposed method with SVs–CHMM based and NSVRs–CHMM based methods, it is demonstrated that SVs and NSVRs both can effectively recognize different bearing fault types. However, the representations of SVs and NSVRs for bearing faults are different. And the combination of SVs and NSVRs is more effective for rolling element bearing fault diagnosis. Furthermore, the probability calculated from CHMM can be used as the index assessing bearing degradation degree. The selected SV–NSVRs and CHMM based bearing performance assessment method is effective when applied to bearing in the accelerated life test. So in conclusion, the proposed method is beneficial for the equipment condition monitoring and maintenance.

## Acknowledgments

The research is supported by the National Natural Science Foundation, China (approved Grant: 51035007 and 51175329). And thanks for the support of Hangzhou Bearing Test & Research Center on bearing accelerated life test.

## Appendix A. The Viterbi algorithm for HMM

The Viterbi algorithm is used to find the most likely state sequence  $Q^*$  that generates a given observation sequence  $O$  [20], which means the most likely state sequence  $Q^*$  meets the condition  $\max_Q P(Q|O, \lambda)$ . Also,  $\max_Q P(Q|O, \lambda)$  is equal to  $\max_Q P(O, Q|\lambda)$ . At first, a variable is defined as

$$\delta_t(i) = \max_{q_1, q_2, \dots, q_{t-1}} P(q_1, q_2, \dots, q_{t-1}, q_t = S_i, o_1, o_2, \dots, o_t | \lambda) \quad (A1)$$

At each time  $t$ , this algorithm computes this variable for each state  $i$ . In summary, the Viterbi algorithm works as follows:

**Step 1: Initialization**

$$\begin{cases} \delta_t(i) = \pi_i b_i(o_{1t}) \\ \psi_1(i) = 0 \end{cases}, \quad 1 \leq i \leq N \quad (\text{A2})$$

**Step 2: Recursion**

$$\begin{cases} \delta_t(j) = \max_{1 \leq i \leq N} [\delta_{t-1} a_{ij}] b_j(o_{tj}) \\ \psi_t(j) = \arg \max_{1 \leq i \leq N} [\delta_{t-1} a_{ij}] \end{cases}, \quad 2 \leq t \leq T, \quad 1 \leq j \leq N \quad (\text{A3})$$

**Step 3: Termination**

$$\begin{cases} P^* = \max_{1 \leq i \leq N} [\delta_T(i)] \\ q_T^* = \arg \max_{1 \leq i \leq N} [\delta_T(i)] \end{cases} \quad (\text{A4})$$

**Step 4: Backtracking**

$$q_t^* = \psi_{t+1}(q_{t+1}^*), \quad t = T-1, \quad t = T-2, \dots, 1 \quad (\text{A5})$$

Then the most likely state sequence  $Q^* = \{q_1^*, q_2^*, \dots, q_T^*\}$  can be found through the backtracking from time  $T-1$  to time 1.

**Appendix B. The Forward–Backward algorithm for HMM**

The Forward–Backward algorithm is used for calculating the probability of the observed sequence when the mode parameters and the observation sequence are given, which can be denoted as  $P(O|\lambda)$ . And in general, the forward algorithm is enough for the calculation of  $P(O|\lambda)$ . However, the forward and backward algorithms are both needed for parameters re-estimation. So both the forward and backward algorithms are introduced as follows:

*B.1. The forward algorithm*

A forward variable is defined as

$$\alpha_t(i) = P(o_1, o_2, \dots, o_t, \quad q_t = S_i | \lambda) \quad (\text{B1})$$

$P(O|\lambda)$  can be calculated through following procedures:

**Step 1: Initialization**

$$\alpha_1(i) = \pi_i b_i(o_{1t}) \quad (\text{B2})$$

**Step 2: Recursion**

$$\alpha_{t+1}(j) = \sum_{i=1}^N \alpha_t(i) a_{ij} b_j(o_{t+1}), \quad 1 \leq t \leq T-1, \quad 1 \leq j \leq N \quad (\text{B3})$$

**Step 3: Termination**

$$P(O|\lambda) = \sum_{i=1}^N \alpha_T(i) \quad (\text{B4})$$

The recursion step is the key procedure of the forward algorithm, of which the illustration is expressed in Fig. B1.

*B.2. The backward algorithm*

A backward variable is defined as

$$\beta_t(i) = P(o_{t+1}, o_{t+2}, \dots, o_T | q_t = S_i, \lambda) \quad (\text{B5})$$

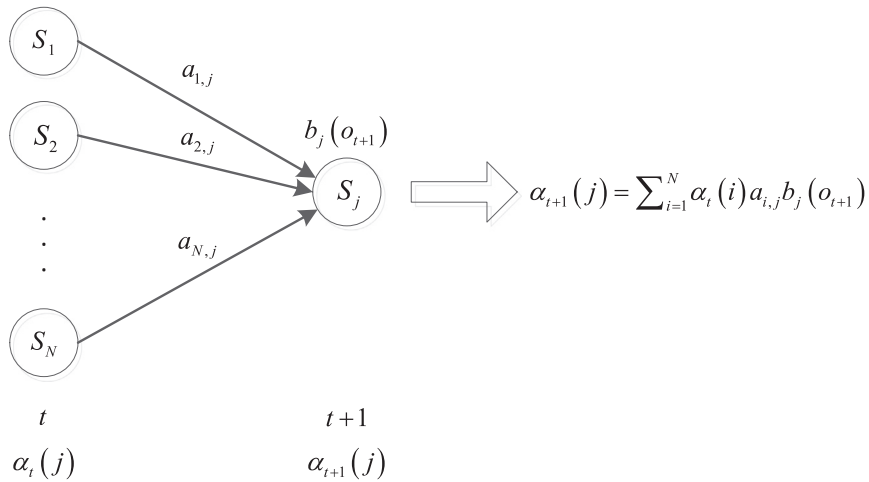


**Fig. B1.** Illustration of the recursive process required for the computation of the forward variable.

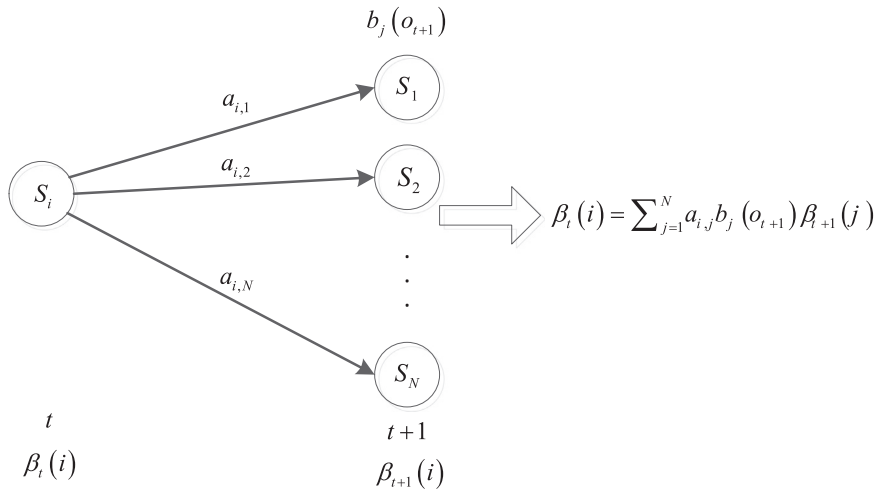


**Fig. B2.** Illustration of the recursive process required for the computation of the backward variable.

The backward variable can be calculated through following procedures:

**Step 1: Initialization**

$$\beta_T(i) = 1, \quad 1 \leq i \leq N \quad (B6)$$

**Step 2: Recursion**

$$\beta_t(i) = \sum_{j=1}^N a_{ij} b_j(o_{t+1}) \beta_{t+1}(j), \quad t = T-1, \quad T-2, \dots, 1, \quad 1 \leq j \leq N \quad (B7)$$

The recursion step is the key procedure of the backward algorithm, and its illustration is shown in Fig. B2. Based on the forward and backward variables,  $P(O|\lambda)$  can be expressed as follows:

$$P(O|\lambda) = \sum_{i=1}^N \alpha_t(i) \beta_t(i). \quad (B8)$$

### Appendix C. The parameter estimation for HMM

#### C.1. The initialization of HMM parameters

The initialization of HMM parameters will affect the performance of the model [41]. The model parameter is  $\lambda=(\pi, A, B)$ . Generally,  $\pi$  and  $A$  have little influence on the final convergence result of the model [20]. So initialize arbitrarily  $\pi$  and  $A$  subjected to Section 3.1. The selection of the hidden states number can refer to the frequently used Bayesian Information Criterion (BIC) and Akaike Information Criterion (AIC) [41]. The initialization of  $B$  influences the model performance a lot. More reliable methods are acquired. The Viterbi algorithm combined with  $k$ -means clustering algorithm is the most widely used method for parameters initialization, which is adopted in this paper. The detailed procedures can be found in reference [50].

#### C.2. The parameter re-estimation for HMM

The iterative algorithm frequently used for parameters re-estimation in HMM-based applications is the Expectation Maximization (EM) algorithm [41]. The EM algorithm was first introduced by Baum and Petrie in 1966 and it was also referred to in the literature as the Baum–Welch algorithm [51]. A variable is defined as

$$\xi_t(i, j) = P(q_t = i, q_{t+1} = j | O, \lambda) \tag{C1}$$

where  $\xi_t(i, j)$  is defined as the probability of being in state  $i$  at time  $t$  and making a transition to state  $j$  at time  $t + 1$ , given the observation sequence and the model  $\lambda$ . And it can be calculated based on the forward variable and the backward variable, as follows:

$$\xi_t(i, j) = \frac{P(q_t = S_i, q_{t+1} = S_j, O | \lambda)}{P(O | \lambda)} = \frac{\alpha_t(i) a_{ij} b_j(o_{t+1}) \beta_{t+1}(j)}{\sum_{i=1}^N \sum_{j=1}^N \alpha_t(i) a_{ij} b_j(o_{t+1}) \beta_{t+1}(j)} \tag{C2}$$

The illustration of  $\xi_t(i, j)$  is shown in Fig. C1. Then similarly, another variable is defined as follows:

$$\begin{aligned} \gamma_t(i) &= P(q_t = S_i | O, \lambda) \\ &= \frac{P(q_t = S_i, O | \lambda)}{P(O | \lambda)} \\ &= \sum_{j=1}^N \xi_t(i, j) \end{aligned} \tag{C3}$$

Using the above formulas,  $\bar{\pi}_i, \bar{a}_{ij}, \bar{b}_j(k)$  of the re-estimated new model can be computed as follows:

$$\bar{\pi}_i = \gamma_1(i) \tag{C4}$$

$$\bar{a}_{ij} = \frac{\sum_{t=1}^{T-1} \xi_t(i, j)}{\sum_{t=1}^{T-1} \gamma_t(i)} \tag{C5}$$

$$\bar{b}_j(k) = \frac{\sum_{t=1}^T \gamma_t(j) \delta(o_t, v_k)}{\sum_{t=1}^T \gamma_t(j)} \tag{C6}$$

In Eq. (C6),  $\delta(x, y)$  is the Dirac function, which is defined as follows:

$$\delta(x, y) = \begin{cases} 1, & x = y \\ 0, & x \neq y \end{cases} \tag{C7}$$

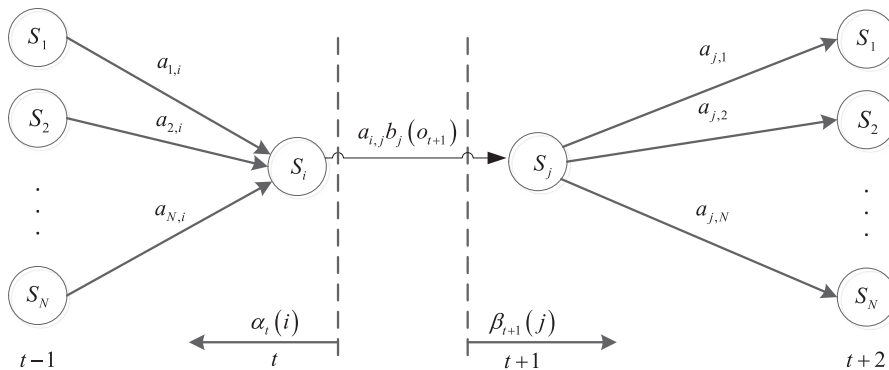


Fig. C1. Illustration of the recursive process required for the computation of variable  $\xi_t(i, j)$ .

Through formulas (C1)–(C6),  $\bar{\lambda} = (\bar{\pi}, \bar{A}, \bar{B})$  is re-estimated. Then  $P(O|\bar{\lambda})$  is calculated. Redo (C1)–(C6), until  $P(O|\bar{\lambda})$  is convergent. And It has been proven by Baum et al. [51] that the iteration leads to the increase of  $P(O|\bar{\lambda})$ .

## References

- [1] N. Tandon, A. Choudhury, A review of vibration and acoustic measurement methods for the detection of defects in rolling element bearings, *Tribol. Int.* 32 (1999) 469–480.
- [2] R.B. Randall, J. Antoni, Rolling element bearing diagnostics – a tutorial, *Mech. Syst. Signal Process.* 25 (2011) 485–520.
- [3] D. Wang, Q. Miao, R. Sun, H.-Z. Huang, Bearing fault diagnosis using singular value decomposition and hidden Markov modeling, in: *Proceedings of the ASME 2009 International Design Engineering Technical Conferences and Computers and Information in Engineering Conference*, American Society of Mechanical Engineers, 2009, pp. 811–817.
- [4] Z. Peng, F. Chu, Application of the wavelet transform in machine condition monitoring and fault diagnostics: a review with bibliography, *Mech. Syst. Signal Process.* 18 (2004) 199–221.
- [5] Y. Pan, J. Chen, X. Li, Bearing performance degradation assessment based on lifting wavelet packet decomposition and fuzzy c-means, *Mech. Syst. Signal Process.* 24 (2010) 559–566.
- [6] P. Kankar, S.C. Sharma, S. Harsha, Fault diagnosis of ball bearings using continuous wavelet transform, *Appl. Soft Comput.* 11 (2011) 2300–2312.
- [7] X. Zhao, T.H. Patel, M.J. Zuo, Multivariate EMD and full spectrum based condition monitoring for rotating machinery, *Mech. Syst. Signal Process.* 27 (2012) 712–728.
- [8] Y. Lei, J. Lin, Z. He, M.J. Zuo, A review on empirical mode decomposition in fault diagnosis of rotating machinery, *Mech. Syst. Signal Process.* 35 (2013) 108–126.
- [9] G. Bin, J. Gao, X. Li, B. Dhillon, Early fault diagnosis of rotating machinery based on wavelet packets – empirical mode decomposition feature extraction and neural network, *Mech. Syst. Signal Process.* 27 (2012) 696–711.
- [10] M. Žvokelj, S. Zupan, I. Prebil, Multivariate and multiscale monitoring of large-size low-speed bearings using ensemble empirical mode decomposition method combined with principal component analysis, *Mech. Syst. Signal Process.* 24 (2010) 1049–1067.
- [11] R. Yan, R.X. Gao, Approximate entropy as a diagnostic tool for machine health monitoring, *Mech. Syst. Signal Process.* 21 (2007) 824–839.
- [12] H. Ocak, Automatic detection of epileptic seizures in EEG using discrete wavelet transform and approximate entropy, *Expert Syst. Appl.* 36 (2009) 2027–2036.
- [13] J.S. Richman, J.R. Moorman, Physiological time-series analysis using approximate entropy and sample entropy, *Am. J. Physiol. – Heart Circ. Physiol.* 278 (2000) H2039–H2049.
- [14] L. Zhang, G. Xiong, H. Liu, H. Zou, W. Guo, Bearing fault diagnosis using multi-scale entropy and adaptive neuro-fuzzy inference, *Expert Syst. Appl.* 37 (2010) 6077–6085.
- [15] X. Zhao, B. Ye, Similarity of signal processing effect between Hankel matrix-based SVD and wavelet transform and its mechanism analysis, *Mech. Syst. Signal Process.* 23 (2009) 1062–1075.
- [16] T. Liu, J. Chen, G. Dong, Singular spectrum analysis and continuous hidden Markov model for rolling element bearing fault diagnosis, *J. Vib. Control* (2013) (in press).
- [17] P. Kanjilal, S. Palit, Modelling and prediction of time series using singular value decomposition and neural networks, *Comput. Electr. Eng.* 21 (1995) 299–309.
- [18] P.P. Kanjilal, S. Palit, On multiple pattern extraction using singular value decomposition, *IEEE Trans. Signal Process.* 43 (1995) 1536–1540.
- [19] F. Cong, J. Chen, G. Dong, F. Zhao, Short-time matrix series based singular value decomposition for rolling bearing fault diagnosis, *Mech. Syst. Signal Process.* 34 (2013) 218–230.
- [20] L. Rabiner, A tutorial on hidden Markov models and selected applications in speech recognition, *Proc. IEEE* 77 (1989) 257–286.
- [21] J.P. Campbell, Speaker recognition: a tutorial, *Proc. IEEE* 85 (1997) 1437–1462.
- [22] T. Varga, H. Bunke, Generation of synthetic training data for an HMM-based handwriting recognition system, document analysis and recognition, in: *Proceedings of the Seventh IEEE International Conference, 2003*, pp. 618–622.
- [23] A. Cohen, Hidden Markov models in biomedical signal processing, in: *Proceedings of the 20th Annual International Conference of the IEEE, Engineering in Medicine and Biology Society, 1998*, pp. 1145–1150.
- [24] T. Williams, X. Ribadeneira, S. Billington, T. Kurfess, Rolling element bearing diagnostics in run-to-failure lifetime testing, *Mech. Syst. Signal Process.* 15 (2001) 979–993.
- [25] S.S.H. Zaidi, S. Aviyente, M. Salman, K.K. Shin, E.G. Strangas, Failure prognosis of DC starter motors using hidden Markov models, in: *Proceedings of the 2009 IEEE International Symposium on Diagnostics for Electric Machines, Power Electronics and Drives, SDEMPED 2009, 2009*, 7 pp.
- [26] Z. Li, Y. He, F. Chu, J. Han, W. Hao, Fault recognition method for speed-up and speed-down process of rotating machinery based on independent component analysis and Factorial Hidden Markov Model, *J. Sound Vib.* 291 (2006) 60–71.
- [27] M. Dong, D. He, A segmental hidden semi-Markov model (HSMM)-based diagnostics and prognostics framework and methodology, *Mech. Syst. Signal Process.* 21 (2007) 2248–2266.
- [28] M. Dong, D. He, Hidden semi-Markov model-based methodology for multi-sensor equipment health diagnosis and prognosis, *Eur. J. Oper. Res.* 178 (2007) 858–878.
- [29] F. Cartella, T. Liu, S. Meganck, J. Lemeire, H. Sahli, Online adaptive learning of Left–Right Continuous HMM for bearings condition assessment, *J. Phys.: Conf. Ser.* 364 (2012) 012031.
- [30] B. Muruganatham, M. Sanjith, B. Krishnakumar, S. Satya Murty, Roller element bearing fault diagnosis using singular spectrum analysis, *Mech. Syst. Signal Process.* 35 (2013) 150–166.
- [31] W. Wang, J. Chen, X. Wu, Z. Wu, The application of some non-linear methods in rotating machinery fault diagnosis, *Mech. Syst. Signal Process.* 15 (2001) 697–705.
- [32] B. Muruganatham, M. Sanjith, B.K. Kumar, S.S. Murty, P. Swaminathan, Inner race bearing fault detection using singular spectrum analysis, in: *Proceedings of the 2010 IEEE International Conference on Communication Control and Computing Technologies (ICCCCT), 2010*, pp. 573–579.
- [33] F. Alonso, D. Salgado, Analysis of the structure of vibration signals for tool wear detection, *Mech. Syst. Signal Process.* 22 (2008) 735–748.
- [34] N. Golyandina, V. Nekrutkin, A.A. Zhigljavsky, *Analysis of Time Series Structure: SSA and Related Techniques*, CRC Press, New York, 2001.
- [35] H. Ocak, K.A. Loparo, A new bearing fault detection and diagnosis scheme based on hidden Markov modeling of vibration signals, in: *Proceedings of the 2001 IEEE International Conference on Acoustics, Speech, and Signal Processing*, vols. I–VI, *Proceedings: vol I: Speech Processing 1; vol II: Speech Processing 2 Ind Technol Track Design & Implementation of Signal Processing Systems Neural Networks for Signal Processing; vol III: Image & Multidimensional Signal Processing Multimedia Signal Processing*, 2001, pp. 3141–3144.
- [36] H. Ocak, K.A. Loparo, HMM-based fault detection and diagnosis scheme for rolling element bearings, *J. Vib. Acoust.* 127 (2005) 299–306.
- [37] H. Ocak, K.A. Loparo, F.M. Discenzo, Online tracking of bearing wear using wavelet packet decomposition and probabilistic modeling: a method for bearing prognostics, *J. Sound Vib.* 302 (2007) 951–961.
- [38] C. Bunks, D. McCarthy, T. Al-Ani, Condition-based maintenance of machines using hidden Markov models, *Mech. Syst. Signal Process.* 14 (2000) 597–612.
- [39] Z. Li, Z. Wu, Y. He, C. Fulei, Hidden Markov model-based fault diagnostics method in speed-up and speed-down process for rotating machinery, *Mech. Syst. Signal Process.* 19 (2005) 329–339.
- [40] Q. Miao, D. Wang, M. Pecht, A probabilistic description scheme for rotating machinery health evaluation, *J. Mech. Sci. Technol.* 24 (2010) 2421–2430.

- [41] Q. Miao, V. Makis, Condition monitoring and classification of rotating machinery using wavelets and hidden Markov models, *Mech. Syst. Signal Process.* 21 (2007) 840–855.
- [42] L.R. Rabiner, A tutorial on hidden Markov models and selected applications in speech recognition, *Proc. IEEE* 77 (1989) 257–286.
- [43] Y. Pan, J. Chen, L. Guo, Robust bearing performance degradation assessment method based on improved wavelet packet – support vector data description, *Mech. Syst. Signal Process.* 23 (2009) 669–681.
- [44] D. Wang, Q. Miao, R. Kang, Robust health evaluation of gearbox subject to tooth failure with wavelet decomposition, *J. Sound Vib.* 324 (2009) 1141–1157.
- [45] D. Wang, W.T. Peter, W. Guo, Q. Miao, Support vector data description for fusion of multiple health indicators for enhancing gearbox fault diagnosis and prognosis, *Meas. Sci. Technol.* 22 (2011) 025102.
- [46] B.-S. Yang, T. Han, J.L. An, ART-KOHONEN neural network for fault diagnosis of rotating machinery, *Mech. Syst. Signal Process.* 18 (2004) 645–657.
- [47] Y. Lei, Z. He, Y. Zi, Q. Hu, Fault diagnosis of rotating machinery based on multiple ANFIS combination with GAs, *Mech. Syst. Signal Process.* 21 (2007) 2280–2294.
- [48] Y. Lei, Z. He, Y. Zi, X. Chen, New clustering algorithm-based fault diagnosis using compensation distance evaluation technique, *Mech. Syst. Signal Process.* 22 (2008) 419–435.
- [49] W.T. Peter, Y. Peng, R. Yam, Wavelet analysis and envelope detection for rolling element bearing fault diagnosis – their effectiveness and flexibilities, *J. Vib. Acoust.* 123 (2001) 303–310.
- [50] J.M. Lee, S.-J. Kim, Y. Hwang, C.-S. Song, Diagnosis of mechanical fault signals using continuous hidden Markov model, *J. Sound Vib.* 276 (2004) 1065–1080.
- [51] L.E. Baum, T. Petrie, G. Soules, N. Weiss, A maximization technique occurring in the statistical analysis of probabilistic functions of Markov chains, *Ann. Math. Stat.* 41 (1970) 164–171.